First-principles modeling hydrogenation of bilayered boron nitride*

Jing Wang(王静), Peng Zhang(张鹏), and Xiang-Mei Duan(段香梅)†

Department of Physics, Faculty of Science, Ningbo University, Ningbo 315211, *China*

(Received 11 January 2016; published online 1 April 2016)

We have investigated the structural and electronic characteristics of hydrogenated boron-nitride bilayer (H–BNBN–H) using first-principles calculations. The results show that hydrogenation can significantly reduce the energy gap of the BN–BN into the visible-light region. Interestingly, the electric field induced by the interface dipoles helps to promote the formation of well-separated electron–hole pairs, as demonstrated by the charge distribution of the VBM and CBM. Moreover, the applied bias voltage on the vertical direction of the bilayer could modulate the band gap, resulting in transition from semiconductor to metal. We conclude that H–BNBN–H could improve the solar energy conversion efficiency, which may provide a new way for tuning the electronic devices to meet different environments and demands.

Keywords: hydrogenated bilayer boron-nitride, photocatalyst, first-principles calculations

PACS: 73.20.At, 74.78.Fk, 71.15.Mb, 71.20.Nr **DOI:** 10.1088/1674-1056/25/5/057301

1. Introduction

Energy is important which guarantees sustainable economic and social development. Nowadays, increasing energy and environmental problems lead to severe challenges for the survival of mankind. From a long-term perspective, solar energy is the only inexhaustible resource to meet the demand. Stimulated by the pioneering work of Fujishima and Honda,[1] which has proved that the photoelectrochemical (PEC) technique can generate hydrogen via water splitting, many efforts have been devoted to search for new photocatalysts that can readily take advantage of abundant sunlight energy to split water into hydrogen. Semiconductor photocatalysis can not only convert solar energy into chemical energy, but also directly degrade and mineralize organic pollutants, which solves the energy shortage and environmental pollution problems, thus showing great potential in artificial photosynthesis.[1–4] Still, most of the photocatalysts are facing the following difficulties: firstly, the band gap is too wide to absorb sunlight efficiently, for instance, titania can only respond to ultraviolet light, which is rarely part of the visible light region;[5–7] secondly, the electric potentials of valence band maximum (VBM) and conduction band minimum (CBM) are very hard to simultaneously meet the needs of reduction and oxidation potentials of water splitting; thirdly, the photo-produced electron–hole pair can easily recombine, which would decrease the catalytic efficiency;[8] lastly, photocatalysts which absorb visible light are not stable during the reaction process, for example, the photo corrosion occurs in CdS.[9] On the whole, both strong light absorption and suitable redox potential are prerequisites for photocatalytic reaction. Recently, 2D layered materials, such as g-C_3N_4,[10–13] graphene/TiO_2,[14,15] g-C_3N_4/MoS_2,[16] and so on, have attractive intensive research interests due to their visible-light-active photo-voltaic properties. From a theoretical point of view, it is needed to further explore new photocatalysts with visible light efficiency, high quantum efficiency, and high stability.

Based on first-principles calculations, Li *et al.*[17] proposed a novel reaction mechanism for water splitting, and proved that, in the near-infrared light region, hydrogen can be produced on a hexagonal boron-nitride (h-BN) bilayer saturated with H and F atoms on each surface. To obtain high optical absorption and high carrier mobility, the concentration and distribution of H and F must be strictly controlled, which may be difficult to achieve in the experiment. Hydrogenation and electric field are well used to tailor the electronic structures of the semiconductors.[11,18] In this paper, we systemically study the geometric and electronic characteristics of h-BN bilayer heterostructure subjected to hydrogenation. We find that the junction has a moderate direct band gap (1.30 eV), and can effectively use the visible light. On the other hand, we also note that the electronic properties of the material can be easily controlled by the external electric field perpendicular to the bilayer, which may provide a new way for tuning the electronic devices to meet different environments and demands. It is intriguing to see that the material can correspondingly switch from semiconductor to conductor.

2. Calculation methods

Our first-principles calculations are based on density functional theory (DFT) with generalized gradient approximation (GGA)[19] for the exchange–correlation potential and Perdew–Burke–Ernzerholf (PBE) functional[19] for the GGA

*Project supported by the National Natural Science Foundation of China (Grant No. 11574167).

†Corresponding author. E-mail: duanxiangmei@nbu.edu.cn

© 2016 Chinese Physical Society and IOP Publishing Ltd

as implemented in the Vienna *ab initio* simulation package (VASP).[20] The interaction between the core and valence electrons is described using the frozen-core projected augmented wave (PAW) approach.[21,22] The dipole correction is applied to compensate the dipole interaction in the direction perpendicular to the plane. We apply periodic boundary conditions with a vacuum space of 30 Å along the z direction in order to avoid the interaction of neighboring junctions. The cutoff energy for the plane-wave basis is set to be 400 eV. Geometry optimizations are carried out until the convergence criterion for the energy ($< 10^{-6}$ eV) is met and the forces on all the atoms are less than 0.01 eV/Å. A Monkhorst–Pack[23] k-mesh of $7 \times 7 \times 1$ is adopted for optimization, while $15 \times 15 \times 1$ is used for the self-consistent energy calculations. Both the lattice constant and the positions of all atoms are allowed to relax using the conjugated gradient method without any symmetric constraints. Since the GGA approach usually underestimates the band gap of a semiconductor, to obtain relatively accurate electronic structures and optical properties, we perform Heyd–Scuseria–Ernzerhof 2006 (HSE06)[24] calculation with the total exchange potential containing 20% of the Hartree–Fock exchange potential. We utilize the imaginary part of the frequency dependent dielectric function to evaluate the optical properties.

The stability of the nanostructures can be defined through the binding energy, which is obtained from the relation

$$E_{\mathrm{b}} = (E_{\mathrm{total}} - n_{\mathrm{B-N}}\mu_{\mathrm{B-N}} - n_{\mathrm{H}}\mu_{\mathrm{H}})/N, \quad (1)$$

where E_{total} is the total energy of the hydrogenated configuration, $n_{\mathrm{B-N}}$ and n_{H} are the numbers of B–N pairs and H atoms, respectively, and N is the total number of atoms. Here, $\mu_{\mathrm{B-N}}$ denotes the chemical potential of a B–N pair, which is the total energy of the h-BN sheet per formula unit; μ_{H} is the chemical potential of a single H atom, which equals to half of the binding energy of an H_2 molecule.

3. Results and discussion

We consider five stacking constructions for BN bilayers, and confirm that the AB stacking structure, with B or N atom sited above the center of the other BN layer, is the lowest in energy among the structures, which agrees well with the previous theoretical results.[25] Considering that the stacking order of the hydrogenated bilayer BN may be affected by the saturated atoms, we check six adsorption sites for hydrogen (see Fig. 1 for the structures), and find that the configuration with AB stacking (denoted as H–BNBN–H) is still the most stable one, thus we focus on this structure in the content below. For the sake of convenience, we mark the two surfaces as the $(00\bar{1})$ and (001) surfaces.

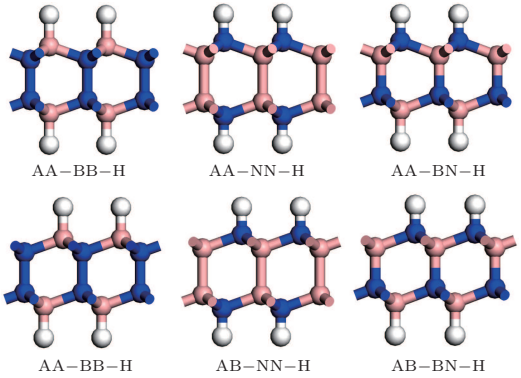


Fig. 1. (color online) Six possible configurations for H saturated on BN bilayers. The blue, pink, and white spheres represent N, B, and H atoms, respectively.

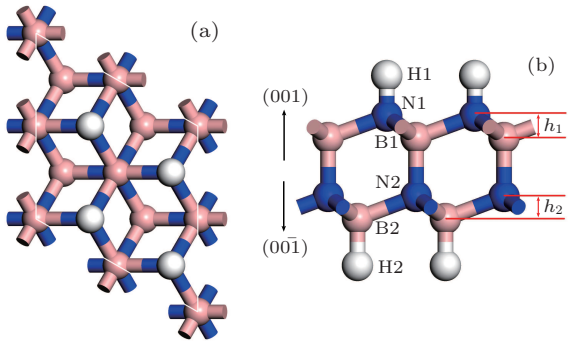


Fig. 2. (color online) (a) Top view and (b) side view of the configuration of H–BNBN–H. The blue, pink, and white spheres represent N, B, and H atoms, respectively.

The optimized structure of H–BNBN–H is shown in Fig. 2, where the lattice parameters equal to 2.59 Å. As a result of the existence of hydrogen atoms, the distance between planes composed of B1 and N1 atoms, h_1, is 0.55 Å, and the distance between planes composed of B2 and N2 atoms, h_2, is 0.56 Å. The interlayer distance (the bond length between B1 and N2) is 1.50 Å, which lies between the B–N bond length (1.45 Å) of BN bilayers and the B–N bond length (1.59 Å) of single layer BN with hydrogenation. The results demonstrate that strong covalent bonds are formed between the two BN layers. The calculated binding energy is –0.23 eV per atom, indicating that the formation of H–BNBN–H is exothermic and stable. Figure 3(a) presents the reaction pathway of H–BNBN–H relative to the two separated H functionalized h-BN layers obtained by the climbing image nudged elastic band method (cNEB).[26,27] It is obvious that there is no energy barrier for the combination of two H–BN and BN–H surfaces. We also check the process for the formation of the hydrogenated BN bilayer, starting with the two flat BN layers (BN-BN) saturated by H, the initial distance between the two H–BN layers is 3.0 Å (the interlayer distance of the BN bilayer before hydrogenation), after the relaxation, the final configuration is H–BNBN–H with the interlayer distance of 1.50 Å. We demonstrate that either the two flat BN monolayers saturated by H, nor the two hydrogenated BN monolayers (see Fig. 3(a)), can

form H–BNBN–H. The band structures in Fig. 3(b) show that H–BNBN–H is a direct band gap semiconductor with both VBM and CBM locating at the Γ point. The band gap with GGA is 0.67 eV, and the value is 1.30 eV with HSE06, corresponding to an adsorption in the visible light region of the solar spectrum.

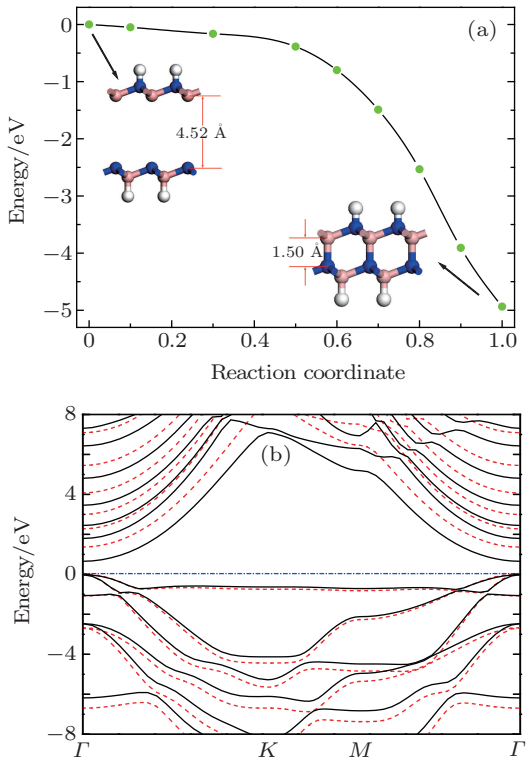


Fig. 3. (color online) (a) The calculated formation reaction pathway of H–BNBN–H from the combination of two functionalized single layers H–BN and BN–H. (b) Band structure of H–BNBN–H. The black solid and red dashed lines represent the GGA and the hybrid HSE06 results, respectively.

Since the junction is asymmetric (shown in Fig. 2) and the electronegativities of the elements (H, B, and N) are different, the rearrangement of electrons at the interface should give rise to a built-in potential difference, which therefore induces an internal electric field by the dipoles at the interface of the $(00\bar{1})$ and (001) surfaces. To better understand the built-in electric field, we plot the spatial charge distributions of VBM and CBM, as shown in Fig. 4. It can be seen that the charge densities of VBM and CBM are effectively separated on the two surfaces. The charge density of VBM is mainly located at N2 atoms in the $(00\bar{1})$ surface, while CBM consists of nearly-free-electron states residing upside of the (001) surface and a minority density at N1 atoms. The plane-averaged electrostatic potential on the CBM is higher than that on the VBM, and it is known that the potential gradually reduces along the direction of the electric field, thus the built-in electric field between the two surfaces forms in the direction pointing from the CBM to the VBM. Therefore, hydrogenation helps to reduce the probability of recombination of photo-generated electrons and holes, and to promote the carrier mobility. Similar behaviors have been reported for H–BNBN–F and semihydroganated BN monolayer.[28] The dipole-induced polarized field is evaluated by the equation

$$E_{\text{eff}} = \frac{P}{\varepsilon_{\text{r}}\varepsilon_0 Sd}, \tag{2}$$

where P is the dipole, ε_{r} is the relative dielectric constant, ε_0 is the permittivity of free space, S is the surface area of the nano-composite, and d is the thickness of the junction. The calculated intrinsic dipole and the electric field are 1.10 Debye and 1.47 V/Å per unit cell, respectively (in comparison, H and F saturated BN bilayer generates a stronger intrinsic dipole of 1.58 Debye and an electric field of about 2.0 V/Å), indicating that the photo-generated carriers are separated automatically.

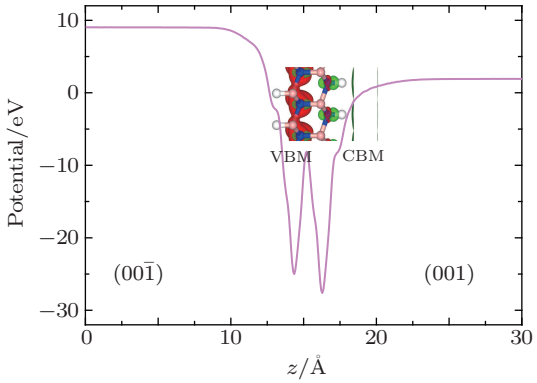


Fig. 4. (color online) Plane-averaged electrostatic potentials along the z direction and the VBM (in red) and CBM (in green) distributions of H–BNBN–H. The calculated electrostatic potential difference of the $(00\bar{1})$ and (001) surfaces.

We perform the Bader analysis[29] of the charge density, and list the results in Table 1. The net charge of H1 and N1 is around -0.30 e and -0.40 e, while the values are about 0.49 e and 0.20 e for H2 and B2, respectively. Thus there is some charge transfer from the (001) surface to the $(00\bar{1})$ surface, resulting in that the holes accumulate in the (001) surface, while the electrons accumulate in the $(00\bar{1})$ surface. These results are consistent with the fact that there exists a polarized field in the junction pointing from the (001) surface to the $(00\bar{1})$ surface.

Table 1. The Bader charge analysis of the optimized H–BNBN–H, comparing to the separated AB stacking BN bilayer and H.

Species	Before hydrogenation	H–BNBN–H	Net charge
H1	1.00	0.70	–0.30
N1	7.15	6.75	–0.40
B1	0.84	0.89	+0.05
N2	7.15	7.11	–0.04
B2	0.84	1.04	+0.20
H2	1.00	1.49	+0.49

The photocatalytic conditions of PEC water splitting are as follows: the oxidation potential on the $(00\bar{1})$ surface should

be higher than the CBM of the semiconductor, while the reduction potential should be lower than the VBM.[6,30] According to the mechanism proposed by Li, once the photocatalyst's band gap is larger than zero, the water splitting reaction can be completed.[17] In the presence of the internal electric field, the potential difference between the oxidation potential on the $(00\bar{1})$ surface and the reduction potential on the (001) surface is decreased from 1.23 eV to 1.23 eV $-\triangle\phi$, where $\triangle\phi$ is the electrostatic potential difference between the two surfaces

$$\triangle\phi = \frac{eP}{\varepsilon_r\varepsilon_0 S}. \tag{3}$$

The electrostatic potential difference is calculated to be 7.1 eV, compared to the value of 10 eV for F–BNBN–H, indicating that the junction is a promising photocatalyst for water splitting.

The spontaneous PEC water-splitting process needs to utilize both the reduction and powers of H–BNBN–H. The oxidation power is measured by the VBM, the lower the VBM energy, the stronger the oxidizing power. The reducing power is evaluated by the CBM, i.e., the closer the CBM to the vacuum level, the stronger the reducing power. We examine the locations of VBM and CBM with respect to the redox potentials of water splitting, and find that the reaction conditions are well satisfied. Figure 5 shows the density of states and schematic energy level diagrams of the junction, we can see that the oxidizing potential for water splitting, $V_{O_2-H_2O}$, is higher than VBM by about 3.38 eV, implying that photogenerated holes can be promptly transferred from the valence band to H_2O, and thus oxidizing it to O_2. The energy location of CBM is 0.63 eV lower than the vacuum energy of the (001) surface, and the reduction potential, $V_{H^+-H_2}$, lies below CBM by 3.81 eV, which indicates that the photo-excited electrons in the conduction band could easily flow down to H_2O or H^+, producing H_2.

The optical properties are calculated by the frequency dependent dielectric function $\varepsilon(\omega) = \varepsilon_1(\omega) + i\varepsilon_2(\omega)$, which is mainly a function of the electronic structure. The imaginary part of the dielectric function, $\varepsilon_2(\omega)$, can be calculated by a summation over empty states using the equation[31]

$$\varepsilon^{(2)}_{\alpha\beta}(\omega) = \frac{4\pi^2 e^2}{\Omega}\lim_{q\to 0}\frac{1}{q^2}\sum_{c,v,k} 2w_k\delta(\varepsilon_{ck}-\varepsilon_{vk}-\omega) \times \langle \mu_{ck}+e_\alpha q|\mu_{vk}\rangle \langle \mu_{ck}+e_\beta q|\mu_{vk}\rangle^*, \tag{4}$$

where the indices c and v refer to conduction and valence band states, respectively, and μ_{ck} is the wave function at the k point. The imaginary part of the dielectric function for H–BNBN–H is shown in Fig. 6; we can see that the material could make full use of visible light. As a result of structural anisotropy, different adsorption behaviors occur in the transversal and longitudinal directions, the imaginary part of the dielectric function in the direction perpendicular to the z axis is much stronger than that in the parallel direction. For a more quantitative picture on the optical property, methods which yield a more accurate description of the band gap, such as GW-BSE,[32–35] would be valuable.

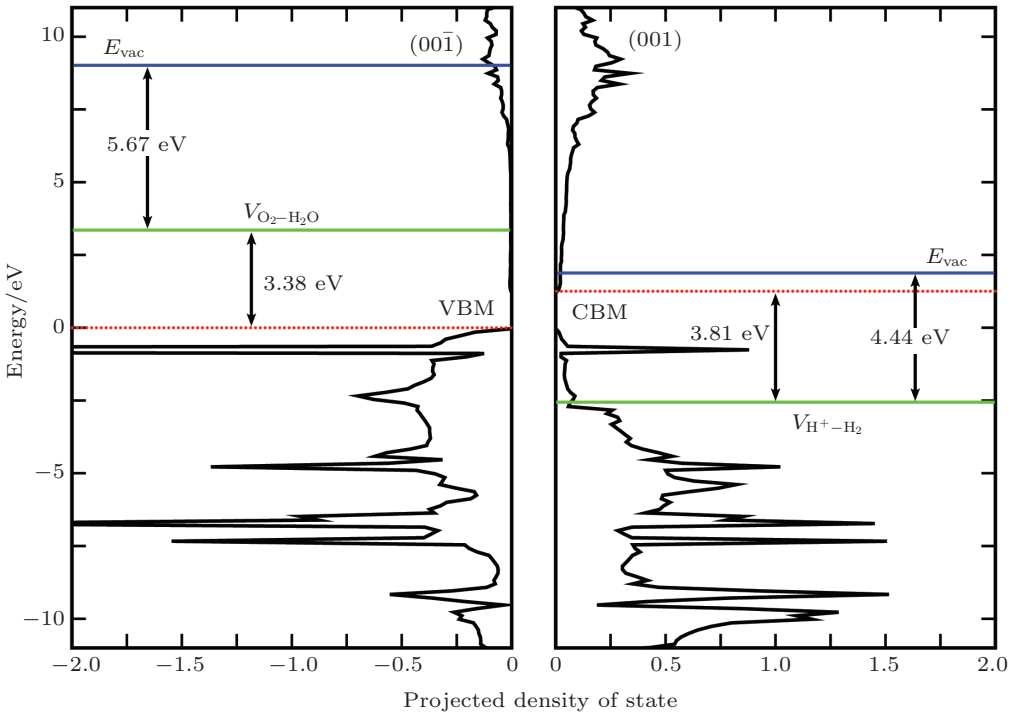


Fig. 5. (color online) Energy diagram of H–BNBN–H. The vacuum level (E_{vac}), redox potentials of water ($V_{O_2-H_2O}$, $V_{H^+-H_2}$), VBM, and CBM are denoted by labeled lines.

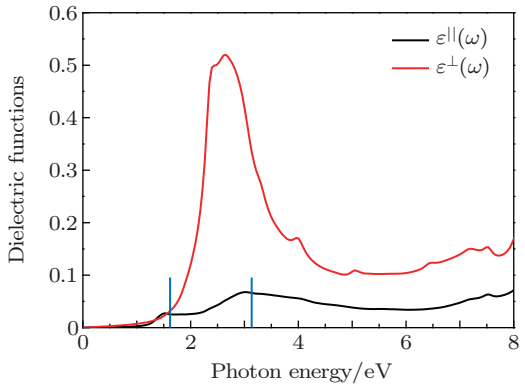


Fig. 6. (color online) The energy-dependent imaginary part of the dielectric function $\varepsilon_2(\omega)$ with the polarization vector parallel and perpendicular to the z axis, where the energy range of visible light is marked by vertical short blue lines.

Generally, the dipole-induced electric field could increase (decrease) the energy of the VBM (CBM) and lead to a relatively small band gap of the junction, it is natural to see whether H–BNBN–H can be tuned by an external electric field. We apply a perpendicular electric field to the junction, and present the response of the material in Fig. 7. Obviously, the energy gap changes monotonically with the external electric field. There exists a critical bias voltage (~ 0.32 eV/Å), when the external electric field exceeds this value, the gap of H–BNBN–H disappears, and the junction exhibits metallic characteristic. Such metallity will block the actual application of polar films. Similar phenomena have been reported for the fully hydrogenated Gr/BN–BC and Gr/Gr–CC.[36]

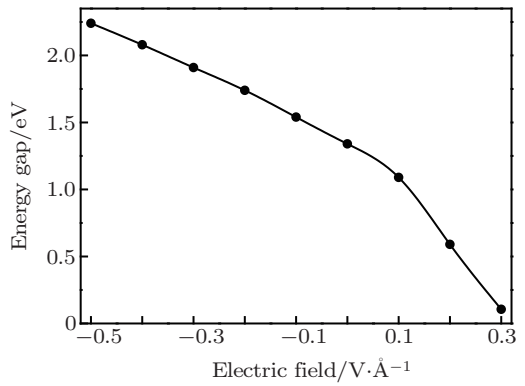


Fig. 7. The calucated energy gap of H–BNBN–H as a function of the external electric field.

4. Conclusion

Based on the first-principles calculation, we have carefully studied the electronic structures and optical properties of the fully hydrogenated bilayered boron nitride, and analyzed the character of the redox reaction. The moderate dipole at the interface plays an important role in the electronic structures of the system. Moreover, as a photocatalysis semiconductor, H–BNBN–H meets the requirement of the water splitting reaction, and the optical absorption edges cover the whole visible light region. The hydrogenated junction is sensitive to the external electric field. In view of the recent progress, our results provide a practical scheme for the photovoltaic materials.

References

[1] Fujishima A and Honda K 1972 *Nature* **238** 37
[2] Maeda K and Domen K 2010 *J. Phys. Chem. Lett.* **1** 2655
[3] Chen X B, Shen S H, Guo L J and Mao S S 2010 *Chem. Rev.* **110** 6503
[4] Hoffmann M R, Martin S T, Choi W and Bahnemann D W 1995 *Chem. Rev.* **95** 69
[5] Wang P, Liu Z R, Lin F, Zhou G, Wu J, Duan W H, Gu B L and Zhang S B 2010 *Phys. Rev. B* **82** 193103
[6] Gai Y Q, Li J B, Li S S, Xia J B and Wei S H 2009 *Phys. Rev. Lett.* **102** 036402
[7] Yin W J, Wei S H, Al-Jassim M M and Yan Y F 2011 *Phys. Rev. Lett.* **106** 066801
[8] Mete E, Uner D, Gülseren O, and Ellialtıoğlu Ş 2009 *Phys. Rev. B* **79** 125418
[9] Kudo A and Miseki Y 2009 *Chem. Soc. Rev.* **38** 253
[10] Ma X G, Lv Y H, Xu J, Liu Y F, Zhang R Q and Zhu Y F 2012 *J. Phys. Chem. C* **116** 23485
[11] Wu F, Liu Y F, Yu G X, Shen D F, Wang Y L and Kan E J 2012 *J. Phys. Chem. C* **3** 3330
[12] Li X R, Dai Y, Ma Y D, Han S H and Huang B B 2014 *Phys. Chem. Chem. Phys.* **16** 4230
[13] Du A J, Sanvito S, Li Z, Wang D W, Jiao Y, Liao T, Sun Q, Ng Y H, Zhu Z H, Amal R and Smith S C 2012 *J. Am. Chem. Soc.* **134** 4393
[14] Du A J, Ng Y H, Bell N J, Zhu Z H, Amal R and Smith S C 2011 *J. Phys. Chem. Lett.* **2** 894
[15] Gao H T, Li X H, Lv J and Liu G J 2013 *J. Phys. Chem. C* **117** 16022
[16] Wang J J, Guan Z Y, Huang J, Li Q X and Yang J L 2014 *J. Mater. Chem. A* **2** 7960
[17] Li X X, Li Z Y and Yang J L 2014 *Phys. Rev. Lett.* **112** 018301
[18] Gao N, Li J C and Jiang Q 2014 *Phys. Chem. Chem. Phys.* **16** 11673
[19] Perdew J P, Burke K and Ernzerhof M 1996 *Phys. Rev. Lett.* **77** 3865
[20] Kresse G and Furthmüller J 1996 *Phys. Rev. B* **54** 11169
[21] Blöchl P E 1994 *Phys. Rev. B* **50** 17953
[22] Kresse G and Joubert D 1999 *Phys. Rev. B* **59** 1758
[23] Monkhorst H J and Pack J D 1976 *Phys. Rev. B* **12** 5188
[24] Heyd J, Scuseria G E and Ernzerhof M 2003 *J. Chem. Phys.* **118** 8207
[25] Zhong X L, Yap Y K, Pandey R and Karna S P 2011 *Phys. Rev. B* **83** 193403
[26] Henkelman G, Uberuaga B P and Jónsson H 2000 *J. Chem. Phys.* **113** 9901
[27] Henkelman G and Jónsson H 2000 *J. Chem. Phys.* **113** 9978
[28] Li X X, Zhao J and Yang J L 2013 *Scientific Reports* **3** 1858
[29] Tang W, Sanville E and Henkelman G 2009 *J. Phys.: Condens. Matter.* **21** 084204
[30] Zhang R Q, Liu X M, Wen Z and Jiang Q 2011 *J. Phys. Chem. C* **115** 3425
[31] Gajdoš M, Hummer K, Kresse G, Furthmüller J and Bechstedt F 2006 *Phys. Rev. B* **73** 045112
[32] Hybertsen M S and Louie S G 1986 *Phys. Rev. B* **34** 5390
[33] Rohlfing M and Louie S G 1998 *Phys. Rev. Lett.* **81** 2312
[34] Benedict L X, Shirley E L and Bohn R B 1998 *Phys. Rev. Lett.* **80** 4514
[35] Albrecht S and Reining L, Del Sole R and Onida G 1998 *Phys. Rev. Lett.* **80** 4510
[36] Cao T F, Zheng X H, Huang L F, Gong P L and Zeng Z 2014 *J. Phys. Chem. C* **118** 10472